Journal of Power Sources 247 (2014) 749–755

Contents lists available at ScienceDirect

Journal of Power Sources

journal homepage: www.elsevier.com/locate/jpowsour

Performance and stability of a liquid anode high-temperature metal–air battery

L. Otaegui [a, *], L.M. Rodriguez-Martinez [b], L. Wang [a, 1], A. Laresgoiti [b], H. Tsukamoto [c], M.H. Han [a], C.-L. Tsai [a, 2], I. Laresgoiti [b], C.M. López [a], T. Rojo [a]

[a] CIC Energigune, Albert Einstein 48, 01510 Miñano, Álava, Spain
[b] IK4-Ikerlan, Energy Business Unit, Juan de la Cierva 1, 01510 Miñano, Álava, Spain
[c] CONNEXX, 912 Regent Park Drive, La Canada Flintridge, CA 91011, USA

HIGHLIGHTS

- A new energy storage device is presented.
- High energy densities are predicted from theoretical estimations.
- Degradation processes are reversible and concept is fully rechargeable.
- Long term stability of the Sn–air battery is demonstrated.

ARTICLE INFO

Article history:
Received 28 May 2013
Received in revised form
26 August 2013
Accepted 6 September 2013
Available online 15 September 2013

Keywords:
Metal–air battery
Molten tin
Liquid metal anode
Oxygen ion conductive electrolyte
Energy storage

ABSTRACT

A High-Temperature Metal–Air Battery (HTMAB) that operates based on a simple redox reaction between molten metal and atmospheric oxygen at 600–1000 °C is presented. This innovative HTMAB concept combines the technology of conventional metal–air batteries with that of solid oxide fuel cells to provide a high energy density system for many applications. Electrochemical reversibility is demonstrated with 95% coulomb efficiency. Cell sealing has been identified as a key issue in order to determine the end-of-charge voltage, enhance coulomb efficiency and ensure long term stability. In this work, molten Sn is selected as anode material. Low utilization of the stored material due to precipitation of the SnO_2 on the electrochemically active area limits the expected capacity, which should theoretically approach 903 mAh g^{-1}. Nevertheless, more than 1000 charge/discharge cycles are performed during more than 1000 h at 800 °C, showing highly promising results of stability, reversibility and cyclability.

1. Introduction

Rechargeable or secondary batteries have been widely used for electronics, stationary and automotive applications. They have been identified as one of the most important enabling technologies in the 21st century due to their significant roles in a green and sustainable energy future. There are many types of rechargeable batteries such as lead-acid, nickel-cadmium, nickel-metal hydride, vanadium redox flow, sodium-sulphur and lithium-ion batteries. Among them, Li-based battery is one of the most advanced and has found widespread applications in the past twenty years. However, current batteries are not keeping up with the demand in terms of energy, power, safety, life and cost. Future batteries will need new chemistries, innovative material concepts, and revolutionary cell designs and manufacturing techniques.

One of the potential systems is metal–air battery such as Li–air or Zn–air. A lithium–air battery typically includes a lithium–metal negative electrode, a positive electrode where reaction with oxygen occurs, e.g. from air, sometimes referred to as an “oxygen positive electrode”, and an electrolyte or other ion conducting medium in fluid communication with both the positive and the negative electrodes. Typically, in non-aqueous systems, lithium and oxygen react to produce lithium peroxide.

On the other hand, solid oxide fuel cells (SOFCs) have been developed as a promising technology that converts the chemical

* Corresponding author. Tel./fax: +34 945 297 108.
E-mail addresses: lotaegui@cicenergigune.com, laidaotaegi@gmail.com (L. Otaegui).
[1] Present address: XG Sciences, 3101 Grand Oaks Drive Lansing, MI 48911, USA.
[2] Present address: Forschungszentrum Jülich GmbH, IEK-1, Germany.

0378-7753/$ – see front matter © 2013 Elsevier B.V. All rights reserved.
http://dx.doi.org/10.1016/j.jpowsour.2013.09.029

energy from a fuel directly into electricity through an electrochemical reaction with oxygen [1]. The major feature of a SOFC is its solid electrolyte which is an oxygen ion conductor. It also has a cathode and an anode where half-cell reactions take place. At the cathode, oxygen is reduced into oxygen ions that are then transported to the anode through the solid electrolyte. At the anode, oxygen ions react with hydrogen-containing fuels to form water, releasing electrons to an external circuit.

Particularly, there is a SOFC that contains a liquid tin layer as part of the anode which can be used for direct power generation from coal or JP8 fuel [2–6]. In such a system, liquid tin fully covers the active oxygen ion exchange area between the electrolyte and the anode and participates as an intermediary for the oxidation of fuel delivered to the fuel cell. In addition, it serves as a buffer against fuel contaminants, as it blocks the transport of insoluble or slag-forming constituents to the electrolyte and impedes the transport of soluble fuel contaminants, thereby reducing the rate of reactions between contaminants and the electrolyte. It is also postulated that the usage efficiency of electrolyte surface is improved over existing porous solid anode technology because the liquid layer fully covers the electrolyte. Hence, oxygen ion reactions can be expected to occur over the full surface of the electrolyte when using a liquid anode, instead of only around triple phase boundaries between the fuel, anode and electrolyte. Jayakumar et al. [7] reported such a device in which Sn and Bi were examined at 973 and 1073 K as anodes in SOFCs with yttria-stabilized zirconia (YSZ) as electrolyte. Although open circuit voltages (OCV) were close to that expected based on their oxidation thermodynamics, their intention was to use molten metal as a medium to transfer oxygen to solid fuels such as coal. Therefore, these systems were still used as energy conversion devices.

Tao et al. [8,9] describe rechargeable devices which have a dual-mode capability. Those devices can operate as a fuel cell and as a battery, and include a liquid metal anode, an electrolyte and a cathode. However, they need to be recharged with a chemical source in order to operate in dual form and only act as a battery for a short period of time when the fuel supply (chemical source) is exhausted or interrupted. Therefore, these systems cannot be considered as pure electric energy storage devices since a chemical reductant is required to reduce the oxidized anode.

Here we propose a metal–air battery [10] in which oxygen ions diffuse through a solid oxide electrolyte between electrodes, where the metal anode works in a melt or semi-melt state, allows the electrochemical reactions to take place and overcomes the problems derived from the use of conventional metal–air batteries. This metal–air battery concept combines the technology of conventional metal–air batteries and SOFCs to provide a high energy storage system for many utility applications. It operates at high temperature, typically between 600 and 1000 °C and uses the cathode and the electrolyte of SOFCs, but metallic fuel is stored as in metal–air batteries. The electrochemical reactions that take place in the new battery system are completely different from those in metal–air batteries or SOFCs as shown in Fig. 1. Contrary to other electrochemical devices that combine the technology of metal–air batteries and solid oxide fuel cells, the HTMAB is only electrically rechargeable and operates as a pure electric energy storage device.

This technology provides a battery system with higher energy density than lithium-ion batteries due to the high specific capacity of metal anodes (i.e. 903 mAh g^{-1} for Sn). Moreover, solid oxide electrolytes prevent short-circuit from happening and are more stable than conventional liquid electrolytes used in Li-ion and Li–air batteries. Volatilization and flammability problems are also

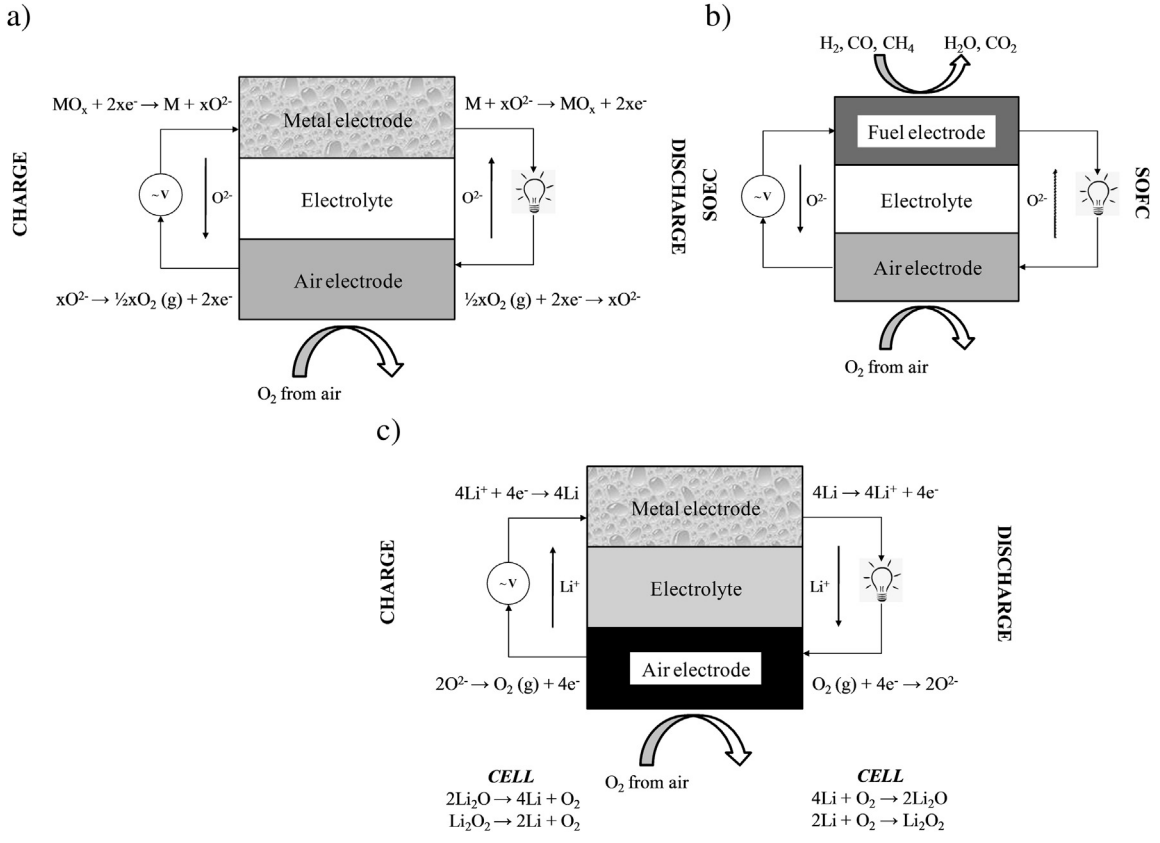

Fig. 1. (a) Electrochemical reactions in HTMABs, (b) SOFCs and (c) lithium–air batteries.

overcome with the choice of solid electrolytes. As an additional advantage, it has a longer cycle life than conventional Li–air cells since no lithium dendrite is formed. Dendrite formation in typical Li-based batteries are widely believed to cause safety problems such as short-circuits and thermal runaway [11,12]. Since the liquid anode prevents the formation of dendrites that might break the electrolyte and "mossy lithium" and active-cation consuming SEI formation are also avoided, the device is considered safer than conventional Li-based batteries in those particular aspects. Because the estimated energy density and the cycle life are larger based on sound theoretical data available, and the used materials are inexpensive (stainless steel, ZrO_2, etc.), the cost per kWh energy is expected to be comparable to, or lower than, the conventional Li-ion or Li–air batteries.

Compared to SOFCs, it uses a stored metal as fuel instead of conventional gaseous fuels and therefore it does not need a fuel distribution system. Operating temperature can be potentially lowered. In addition, the power density per unit area is much higher.

In this paper we report the first proof of concept for the HTMAB using Sn as a molten anode, composite $(La_{0.6}Sr_{0.4})_{0.95}FeO_{3-x}$–$Ce_{0.8}Sm_{0.2}O_{2-x}$ (LSF–SDC) as a cathode, and O^{2-} ion conducting $(ZrO_2)_{0.97}(Y_2O_3)_{0.03}$ (3YSZ) as solid electrolyte. The proof is presented in terms of reversibility, electrical rechargeability, compatibility amongst concept components at 800 °C and promising stability. The theoretical specific capacity of Sn and other anode materials are also included and compared to the experimental data obtained in this work.

2. Experimental

In a typical HTMAB cell, a 300 μm thick yttrium doped zirconia (3YSZ) electrolyte disc (Kerafol) was used to deposit a LSF–SDC (70/30 wt%) composite cathode material (Nextech Materials). Pt paste was used as cathode current collector and a piece of Pt mesh was attached across the cathode area using Pt paste for electrical connection. Cathode and current collector were fired at 950 °C for 2 h in air. The electrolyte-cathode system was then sealed to an alumina inert testing tube using ceramic sealant (Aremco). The anode material, *ca.* 9 g of solid Sn (Alfa Aesar), was placed inside the alumina tube over the free side of the electrolyte. The theoretical capacity for the amount of stored anode material is expected to be 4148 mAh cm^{-2}. A passivated/coated metallic anode current collector (commercial ferritic steel, ThyssenKrupp VDM), welded to Pt wires was then placed inside the tube. Protective gas (Ar) was introduced into the anode side while the system was heated up to operation temperature at 800 °C to prevent the oxidation of the anode, therefore the cell started in the charged state. Once the system reached 800 °C, the current collector was introduced into the molten anode (m.p of Sn = 232 °C) and the discharge/charge operation started under the inert gas atmosphere in the anode side. The charge/discharge cycles were recorded with Bio-Logic VMP3 potentiostat equipped with electrochemical impedance spectroscopy capability, at current densities in the range from 5 to 50 mA cm^{-2}. Cut-off potentials were set at 0.96 and 0.7 V respectively for charge and discharge. Post-test analyses were conducted using FEI Quanta 200 FEG SEM both on anode surfaces and embedded cross sections.

3. Results and discussion

3.1. Theoretical HTMAB concept performance

Currently, the state-of-art lithium–ion batteries have a gravimetric energy density of 100–200 Wh kg^{-1} or 300–500 Wh l^{-1} depending on applications. The energy density forecast for this system, is summarized in Table 1. These values were estimated based on the preliminary design parameters described below considering 100% anode utilization. Future developments will give a much more realistic perspective of this new technology.

Key parameters for the modelling are: type of metal fuels, electrochemical reactions, the theoretical cell voltage of the systems, dimensions of the electrodes and electrolyte and a factor of other components which include sealing, current collector and packaging. The cell voltage for each metal was calculated based on Gibbs free energy of formation of their corresponding oxides [13] when referenced to air. Oxygen ions generated at the cathode from atmospheric air were used together with different metallic anodes and assembled in either a tubular design with 5 mm diameter and 18 cm long ceramic tube or a planar cell of 20 × 20 cm^2. For the initial calculations, $La_{0.7}Sr_{0.3}CoO_x$ (density ≈5 g cm^{-3}) was chosen as cathode material (assuming 30% porosity and 30 μm thickness). YSZ (density ≈6 g cm^{-3}) was used both as ceramic anode matrix (50% porosity) and dense electrolyte (30 μm thick). Metal anode density at 800 °C was used for the calculations. The density of the metals at 800 °C is lower than that at room temperature; therefore, the anode volume will increase when the cell is heated up to operating temperature. In order to avoid cell failure due to the volume expansion of the anode, the more conservative density values were selected. The current collector was a 10 μm thick dense ferritic stainless steel (density = 8.9 g cm^{-3}).

A "packing factor" of 0.5 was assumed, which means that the real weight and volume of the battery are twice as much as those of individual cells. In another words, it was assumed that sealing, interconnection, packaging and others contribute to 50% of the total battery weight and volume. This "packing factor" can be readjusted later based on practical data.

As a result of preliminary estimations in Table 1, for the proposed metal–air battery, the goals for energy density are expected >250 Wh kg^{-1} or 800 Wh l^{-1}. Particularly, Mg is expected to accomplish specific energy target for planar designs while Li and Zn will also do it when tubular designs are used. Energy densities higher than 800 Wh l^{-1} are expected when Li, Sn, Mg and Zn are used as anode materials for both tubular and planar designs. Since

Table 1
Theoretical specific capacities and energy densities of different metal–air systems using tubular and planar designs at 800 °C operating temperature.

Metal	Reaction at 800 °C	Metal density (g cm^{-3})	Cell voltage (V)	Energy density (tubular design)		Energy density (planar design)	
				(Wh kg^{-1})	(Wh l^{-1})	(Wh kg^{-1})	(Wh l^{-1})
Li	$2Li + 0.5O_2 \leftrightarrow Li_2O$	0.45 [14]	2.34	294	1015	227	823
Na	$2Na + 0.5O_2 \leftrightarrow Na_2O$	0.78 [15]	1.37	86	311	67	252
Sn	$Sn + O_2 \leftrightarrow SnO_2$	6.60 [16]	0.90	205	1338	177	1085
Mg	$Mg + 0.5O_2 \leftrightarrow MgO$	1.55 [17]	2.47	527	2108	420	1710
Zn	$Zn + 0.5O_2 \leftrightarrow ZnO$	6.25 [18]	1.23	248	1578	214	1280

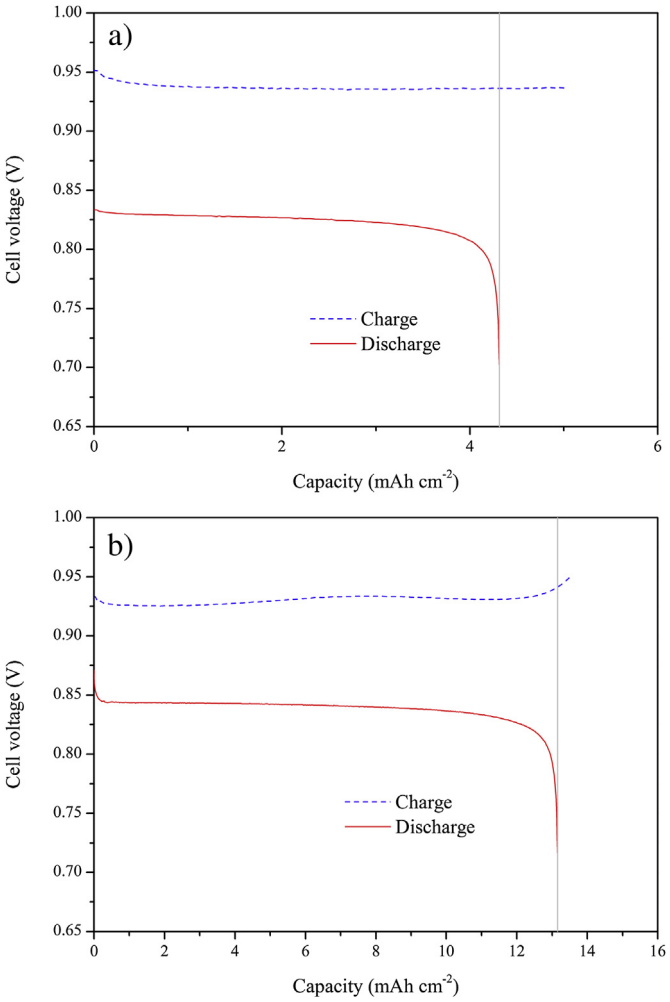

Fig. 2. (a) A typical charge/discharge curve for cells with poor sealing. The discrepancy between charge and discharge curve is due to poor sealing. (b) Charge/discharge curve of the cell with improved sealing.

YSZ electrolyte is not thermodynamically stable in contact with some of the metal anodes that achieve the energy density goals (i.e. Li and Mg), the use of alternative electrolyte materials might be necessary to come closer to the stated targets.

3.2. Electrochemical characterization of HTMAB concept cells

Fig. 2(a) shows the typical cycling behaviour of initial HTMAB cells cycled at a current density of 10 mA cm^{-2}. Open circuit voltage of the cell was 0.88 V, close to the theoretical potential for the oxidation of Sn to SnO_2 at 800 °C, which is 0.90 V when referenced to air (pO_2 = 0.21). The cell delivered a discharge capacity of 4.3 mAh cm^{-2}. However, charge capacity was larger than that of discharge capacity, implying coulomb efficiency lower than 100%. This discrepancy is attributed to an initially poor sealing which enabled the formation of additional SnO_2 when O_2 penetrated through the deficiently sealed areas between the alumina tube and the electrolyte to directly oxidize Sn. The continuous air source leads to a flat charge curve without evidence of reaching the end-of-charge voltage.

Experimental designs and ceramic sealants applied in between the alumina tube and the electrolyte were progressively optimized to eliminate air leakage into the anode chamber. Under the same conditions used in the test of Fig. 2(a), charge/discharge curves of the new cell with better sealing are shown in Fig. 2(b), which exhibit little discrepancy between charge and discharge capacity, indicative of the role of the sealing in improving the electrochemical performance. The redox process of the new cell is solely due to the electrochemical reaction between the molten metal and O^{2-} from the electrolyte, without any additional oxygen supply from external sources that would directly oxidize the metal. Therefore, a sharp increase in cell voltage which allows the determination of the end-of-charge was observed and was set at 0.96 V in the subsequent long term stability tests. Higher voltages were rejected in order to prevent the reduction of the protective layer of the anode current collector. Coulomb efficiency for this cell is 95% which reflects a highly promising electrochemical reversibility for the HTMAB concept.

Table 2
Electrochemical performances for different tested cells.

Cell no.	OCV (V)	R_Ω (Ω)	Discharge capacity (mAh cm^{-2})
1	0.88	–	4.3
2	0.89	3.5	11.3
3	0.90	1.3	10.2
4	0.90	0.9	13.2

Table 2 shows the evolution of relevant electrochemical data recorded while improving cell sealing. The charge/discharge curves represented in Fig. 2(a) and (b) correspond to cells #1 and #4 in Table 2, respectively. The OCV of all the tested cells was almost identical to the theoretical value. Ohmic resistance across the cells measured in charged state progressively decreased from 3.5 to 0.9 Ω as a direct consequence of successful sealing. The ohmic resistance of 0.9 Ω obtained for the best cell is close to the expected resistance for a 300 μm thick 3YSZ electrolyte at 800 °C, based on reported conductivity, 0.016 S cm^{-1} [19]. This indicates that the ohmic losses can be attributed mostly to the electrolyte when complete sealing is achieved, with anode current collector contribution being nearly negligible. However, when sealing is deficient, the formation of SnO_2 occurs all over the exposed Sn surface, including the anode/current collector interface. The contribution in the ohmic resistance of this SnO_2 layer is significant comparing to that of the electrolyte. Discharge capacity also triples for the cells with improved sealing.

The appearance of Sn surfaces in contact with the electrolyte for cells #1 and #4 after cycling are shown in Fig. 3. The smooth metallic regions correspond to metal Sn and the rugged white areas are SnO_2. The electrochemically active area, 1.96 cm^2, is limited by the cathode area and is indicated by dashed lines. Metallic Sn oxidized by air which leak through the sealant is evident in Fig. 3(a). The images, therefore, confirm the differences in sealing quality between the cells, which is in agreement with the results from electrochemical characterization.

The presence of SnO_2 in the electrochemically active area affected the capacity due to the reduction of the active area available for electrochemical reaction. On the other hand, the formation of SnO_2 on the anode/current collector interface lead to a higher ohmic resistance. On the contrary, limited oxide formation was observed in the active area in Fig. 3(b). Only a small portion of SnO_2 was found on the left hand side of the image, outside from the electrochemically active region, and two lines (marked with dashed arrows) that were attributed to two cracks formed in the electrolyte during the cooling process. The absence of SnO_2 in the electrochemically active area and on the anode/current collector interface gave rise to the significant improvement of delivered capacity as well as ohmic resistance for cell #4.

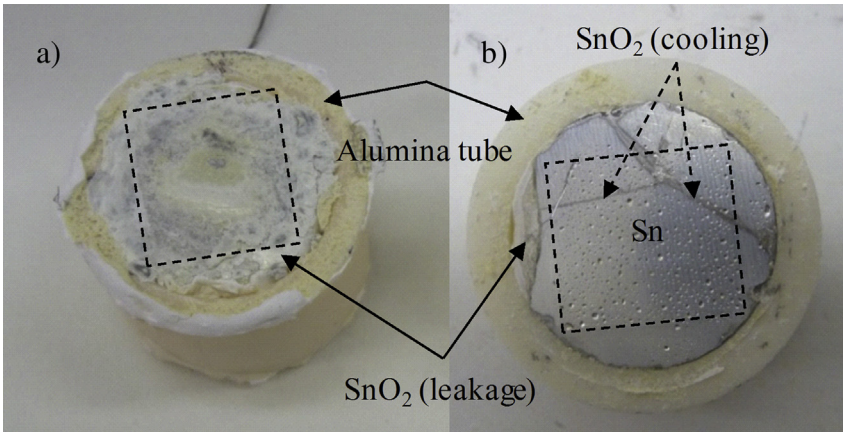

Fig. 3. Images of Sn surfaces which were in contact with the electrolyte. The metallic part is Sn and the white powder corresponds to SnO_2. The square in dashed lines indicates the active area. (a) Cell #1 with deficient sealing and (b) #4 with improved sealing system.

3.3. Microstructural characterization of HTMAB concept cell

To further investigate the formation and reduction of SnO_2, post-test analysis of three different cells with improved sealing was performed for both charged and discharged states. Cells were cycled under constant current density, 10 mA cm^{-2}, and the cell's cut-off voltages were set at 0.7 and 0.96 V. Fig. 4(a) and (b) are SEM images of the anode at the interface between Sn and the YSZ electrolyte, corresponding to two different cells. The first cell was cooled down after the first full discharge, and the second one after the first full cycle. Fig. 4(c) shows the anode/electrolyte interface of a third cell, cooled down after the second full discharge. Dark grey particles are SnO_2 and light grey areas metallic Sn according to EDS analysis.

At first full discharging, Fig. 4(a), the anode surface in contact with the electrolyte was mainly dominated by SnO_2 which was formed as clusters of particles with sizes ranging from approximately 70–230 μm. Randomly distributed small areas of Sn are mainly a consequence of the poor contact between the molten metal and the electrolyte that impedes O^{2-} diffusion and further oxidation of Sn. However, they can be also attributed to the voids left over by SnO_2 particles that are attached to the electrolyte when it is removed for cell disassembly. The cell in Fig. 4(b) was considered to be fully charged at this stage. This means that all the SnO_2 should have been electrochemically reduced into Sn. However, some SnO_2 remained on the active area, indicating that the charge was not completed. It suggests that the end-of-charge might be more efficiently obtained with other charging methods (e.g. constant current–constant voltage method, higher end-of-charge voltage, etc). At the second full discharge, Fig. 4(c), the surface turns back to SnO_2. This second discharge surface has more SnO_2 than the first one, which may possibly be due to the accumulation of oxides that were not reduced efficiently during the previous charging process or variations from cell to cell.

A thin layer of SnO_2 was formed throughout the interface between anode and electrolyte as shown in Fig. 5(a) and (b), that correspond to the cross sections of the fully discharged cells shown in Fig. 4(a) and (c) respectively. At the operating temperature, 800 °C, tin oxide is solid and its density is higher than that of molten tin (6.98 and 6.6 g cm^{-3} for SnO_2 and Sn, respectively [16]). As a consequence of the planar configuration of the cell, with the molten metal on top of the electrolyte, the created SnO_2 remained over the electrolyte and blocked the O^{2-} diffusion path for further oxidation of metallic Sn. The blockage of O^{2-} diffusion path combined with the poor wetting between Sn and YSZ lead to a very small usage of the available anode. Therefore, the discharge capacity was much lower than the expected for the amount of anode material stored in the battery and predicted in preliminary design modelling in Section 3.1. Improving the wettability between the anode material and the solid electrolyte as well as seeking for more suitable materials to increase the anode utilization are under investigation. In this regard, metals or alloys that are denser than their corresponding oxides, as well as those that form oxygen ion conducting oxides are the most promising candidates.

The anode material utilization and the thickness of the created oxides were determined in two different ways. Theoretical thicknesses and anode material utilization were calculated by using the charge transformation over the discharge process for the cells presented in Fig. 5(a) and (b). Formation of a continuous SnO_2 layer was assumed in this calculation and calculated thicknesses were

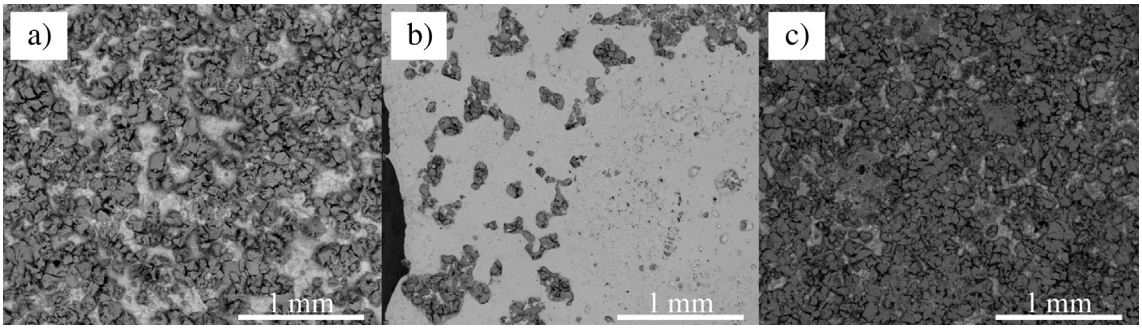

Fig. 4. SEM images of Sn surfaces which were in contact with electrolyte. Cell after (a) first full discharge, (b) first full cycle, and (c) second full discharge.

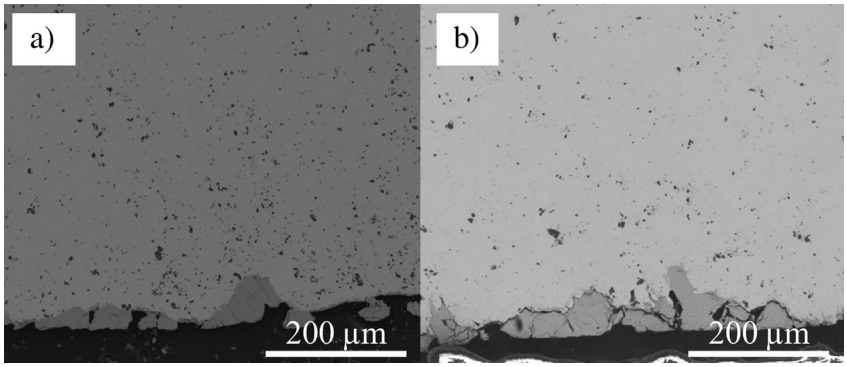

Fig. 5. Cross-section of the cells interface between Sn and YSZ. Cell after (a) first full discharge, (b) second full discharge.

22.93 and 17.27 µm. Accordingly, only a small portion of metal Sn was effectively used during the reactions (0.027 and 0.025 g, i.e. 0.31 and 0.28%). SnO_2 thickness was also directly measured from SEM images of the cross sections (Fig. 5(a) and (b)). In each sample, 5 images from different zones were taken and 25 different points were randomly picked in each image for the average thickness calculation which gave 65 ± 25 µm. The measured thickness was much higher than those values calculated based on discharge capacity which could be attributed to the non-homogeneous formation of the oxides. As shown in Figs. 4 and 5, SnO_2 is formed in discrete particles and not as a continuous layer all over the anode/electrolyte contact area, which made theoretical calculations to provide lower thicknesses than real.

3.4. Long term stability of HTMAB cell concept

Charge–discharge cycles were performed at 800 °C for cells #1 and #4 to analyze the cell cycling behaviour and the influence of sealing quality in performance stability. Applied current density was 10 mA cm^{-2} in both cases. Since the end-of-charge voltage could not be defined for cell #1, it was charged for 30 min, which corresponded to the approximate first discharge capacity. The end-of-charge voltage was set at 0.96 V for cell #4. Both cells were discharged until 0.7 V, where more than 99% of the complete discharge capacity was achieved.

Cell #1 demonstrated electrochemical reversibility with 70–90% coulomb efficiency over 45 cycles in Fig. 6(a). The unstable cycling behaviour is attributed to the deficient sealing that caused uncontrollable amount of oxygen from air to directly oxidize metallic Sn into SnO_2. Consequently, as the amount of non-electrochemically created oxides changes in every new cycle, the discharge capacity varies proportionally. Being that the charge capacity was held constant, variations in coulomb efficiency corresponded only to those variations in discharge capacity.

In addition to the influence in initial cell performance that was previously analyzed in Section 3.2, sealing quality also had significant impact in performance stability. Fig. 6(b) represents the capacity and coulomb efficiency for cell #4 with improved sealing. An initial coulomb efficiency of 95% remained almost unaltered for more than 100 cycles. However, the capacity progressively decreased as a consequence of accumulation of electrochemically created SnO_2 that is not reduced in the recharge processes when end-of-charge voltage is set at 0.96 V as observed in Fig. 4(b).

After initial cycles at a constant current density of 10 mA cm^{-2}, cell #4 was extensively cycled under different current densities ranging from 5 to 50 mA cm^{-2} for more than 1000 cycles. The outstanding electrochemical reversibility of this type of HTMAB has never been reported to our knowledge. The main objective of this preliminary long term test was to evaluate the potential durability of the new HTMAB concept. The influence of applied current density load in delivered capacity and efficiency was also analyzed. Delivered capacity and coulomb efficiency are represented in Fig. 7. In this graph, first 20 cycles correspond to initial conditioning tests and subsequent 100 cycles under a current load of 10 mA cm^{-2} are those expanded in Fig. 6(b).

The effect of applying different current density loadings resulted to be significant. When applied current density was increased to 50 mA cm^{-2}, the cell delivered lower capacity while coulomb efficiency was almost 100%. When redox rate by electrochemical

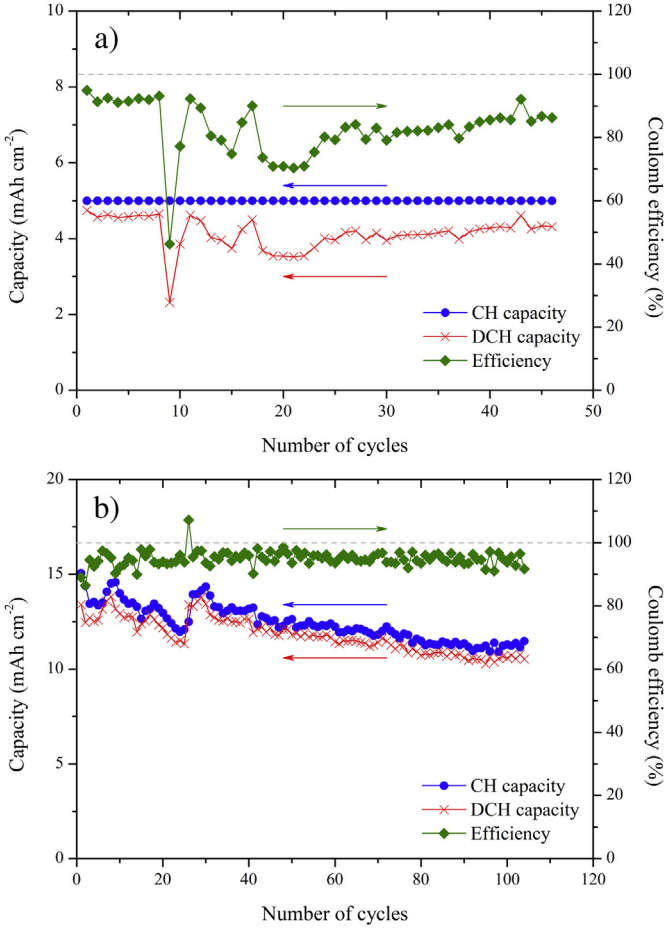

Fig. 6. (a) Specific capacity and coulomb efficiency for cell #1 over 45 cycles. (b) Specific capacity and coulomb efficiency for the cell #4 over 100 cycles.

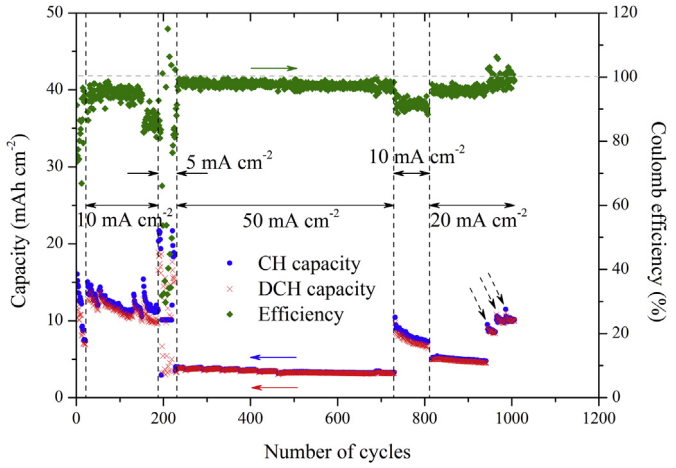

Fig. 7. Specific capacity and coulomb efficiency for cell #4 over 1000 cycles in different charge/discharge regimes.

process is higher than that of oxygen leakage, it enables total utilization of the charged capacity and thus high coulomb efficiencies can be achieved. On the other hand, O^{2-} ions are faster piled up in the electrolyte/anode interface due to the diffusion limitation through the SnO_2 layer, leading to the cut-off potential earlier than that for lower current rates and a decrease of the delivered capacity. Oscillations in both capacity and coulomb efficiency, similar to those observed for cell #1 in Fig. 6(a), occur when applied a current density of 5 mA cm^{-2}. This evidences that the oxygen leakage that is not significant at high current densities becomes relevant at lower current density loads, which decreases coulomb efficiency. This phenomenon suggests that sealing still needs further improvements.

At the final part of the long term test, marked with dashed arrows in Fig. 7, three longer charges with the end-of-charge voltage set at 1.5 V were performed with the aim of regenerating the cell. Under these charging conditions, the remaining SnO_2 from incomplete charging or leakage could be reduced which led to the recovery of both delivered capacity and coulomb efficiency after more than 1000 cycles. This suggests that degradation processes can be recovered by applying proper electrochemical treatment of the cell, showing highly promising results for using the new HTMAB concept in energy storage applications. Besides, it is worth mentioning that other cell components also showed excellent long term stability. LSF-SDC cathode operated under reversible conditions and showed no evidence of performance degradation. The ferritic anode current collector had neither corroded nor formed alloy with liquid tin after immersed in liquid tin for more than 1000 h at 800 °C. These outstanding results in terms of reversibility and stability made possible the fabrication of first prototypes of Sn-cells that were successfully tested and will be published elsewhere.

4. Conclusion

The innovative high-temperature metal–air battery concept (HTMAB) has been successfully demonstrated using liquid Sn as anode, YSZ as electrolyte and LSF–SDC as cathode components. According to our preliminary theoretical calculation, energy densities higher than 250 Wh kg^{-1} or 800 Wh l^{-1} are expected depending on anode material and cell design. However, the energy density of the cell using Sn as anode material is significantly lower due to the poor wetting between the anode material and the electrolyte and the blockage of the O^{2-} diffusion path in the anode by the discharged product, SnO_2. SEM analysis of discharged cells and theoretical calculations based on delivered capacity demonstrate that only a little amount of the stored anode material was used in the electrochemical reaction. Further research on improving anode utilization is currently under development.

Cell performance is also limited by the leakage of air that permits additional formation of SnO_2 on the electrochemically active area and the anode/current collector interface. It therefore reduces the available sites for electrochemical reaction and increases ohmic resistance due to the low conductivity of the formed oxides. The improving of system sealing allowed us to estimate the end-of-charge voltage, increase delivered specific capacity by a factor of 3 and enhance the coulomb efficiency. SEM analysis of charged cells showed that some SnO_2 remained on the electrochemically active area even when cells were charged until 0.96 V, resulting in a reduction of cell capacity over cycling. Nevertheless, the degradation of the cell specific capacity can be recovered after more than 1000 cycles during 1000 h to the initial values by increasing the end-of-charge voltage, demonstrating the excellent electrochemical reversibility of this battery.

Acknowledgements

This work was supported by the ETORTEK program of the Basque Government and CIC Energigune.

References

[1] A. Boudghene Stambouli, E. Traversa, Renew. Sustain. Energy Rev. 6 (2002) 297–306.
[2] T. Tao, in: 9th International Symposium on Solid Oxide Fuel Cells, SOFC IX, 2005, pp. 353–362.
[3] T.T. Tao, W.A. McPhee, M.T. Koslowske, L.S. Bateman, M.J. Slaney, J. Bentley, ECS Trans. 12 (1) (2008) 681–690.
[4] W.A.G. McPhee, M. Boucher, J. Stuart, R.S. Parnas, M. Koslowske, T. Tao, B.A. Wilhite, Energy and Fuels 23 (2009) 5036–5041.
[5] M.T. Koslowske, W.A. McPhee, L.S. Bateman, J.J. Slaney, J. Benley, T.T. Tao, in: Advances in Solid Oxide Fuel Cells V – 33rd International Conference on Advanced Ceramics and Composites, 2010, pp. 27–35.
[6] T.T. Tao, W. McPhee, M. Koslowske, J. Bentley, M. Slaney, L. Bateman, ECS Trans. 25 (2) (2009) 1115–1124.
[7] A. Jayakumar, S. Lee, A. Hornés, J.M. Vohs, R.J. Gorte, J. Electrochem. Soc. 157 (3) (2010) B365–B369.
[8] T.T. Tao, W. Bai, S. Rackey, G. Wang, International Patent Application, WO 03/001617, 2003.
[9] T.T. Tao, W. Bai, International Patent Application, WO 01/80335, 2001.
[10] L. Wang, L.M. Rodriguez-Martinez, A. Laresgoiti, L. Otaegui, H. Tsukamoto, European Patent Application, EP11382390.0, 2011.
[11] C.M. López, J.T. Vaughey, D.W. Dees, J. Electrochem. Soc. 156 (9) (2009) A726–A729.
[12] C.M. López, J.T. Vaughey, D.W. Dees, J. Electrochem. Soc. 159 (6) (2012) A873–A886.
[13] H.J.T. Ellingham, J. Soc. Chem. Ind. 63 (1944) 125.
[14] E.I. Goltsova, High Temperature 4 (1966) 348.
[15] N.B. Vargaftik, V.F. Kozhevnikov, V.A. Alekseev, in: R.W. Ohse (Ed.), Handbook of Thermodynamic and Transport Properties of Alkali Metals, Blackwell Scientific, Oxford, 1985, p. 485.
[16] H. Abernathy, R. Gemmen, K. Gerdes, M. Koslowske, T. Tao, J. Power Sources 196 (2011) 4564–4572.
[17] P.J. Mcgonigal, A.D. Kirshenbaum, A.V. Grosse, J. Phys. Chem. 66 (4) (1962) 737–740.
[18] R. Schuhmann, H.W. Schadler, in: C.H. Mathewson (Ed.), The Science and Technology of the Metal, Its Alloys and Compounds, Reinhold Publishing Corporation, New York, 1959, pp. 65–102.
[19] A. Weber, E. Ivers-Tiffée, J. Power Sources 127 (2004) 273–283.